Mon. Not. R. Astron. Soc. **000**, 000–000 (0000) Printed 7 August 2018 (MN LATEX style file v1.4)

Asymmetry of jets, lobe length and spectral index in quasars

J. Dennett-Thorpe,[1⋆] A. H. Bridle,[2] P. A. G. Scheuer,[1]
R. A. Laing [3] and J. P. Leahy [4]

[1] *Mullard Radio Astronomy Observatory, Cavendish Laboratory, Madingley Road, Cambridge CB3 0HE*
[2] *National Radio Astronomy Observatory, 520 Edgemont Road, Charlottesville VA 22903-2475, USA*
[3] *Royal Greenwich Observatory, Madingley Road, Cambridge CB3 0EZ*
[4] *Nuffield Radio Astronomy Observatories, Jodrell Bank, Macclesfield, Cheshire SK11 9DL*

Received

ABSTRACT

The less depolarized lobe of a radio source is generally the lobe containing the jet (Laing-Garrington correlation) but the less depolarized lobe is also generally that with the flatter radio spectrum (Liu-Pooley correlation). Both effects are strong; taken together they would imply a correlation between jet side and lobe spectral index, i.e. between an orientation-dependent feature and one which is intrinsic. We test this prediction using detailed spectral imaging of a sample of quasars with well-defined jets and investigate whether the result can be reconciled with the standard interpretation of one-sided jets in terms of relativistic aberration. Our central finding is that the spectrum of high surface brightness regions is indeed flatter on the jet side, but that the spectrum of low surface brightness regions is flatter on the side with the longer lobe. We discuss possible causes for these correlations and favour explanations in terms of relativistic bulk motion in the high surface brightness regions and differential synchrotron ageing in the extended lobe material.

Key words: galaxies: jets – quasars: general – radio continuum: general

1 INTRODUCTION

1.1 The problem

Laing, Garrington and colleagues (Garrington et al. 1988; Laing 1988) showed that the lobe of a powerful radio source containing the jet is almost invariably less depolarized than its counterpart on the opposite side of the nucleus; 39 out of the 47 sources in Tables 3 to 6 of Garrington, Conway & Leahy (1991) obey the Laing–Garrington rule (only 4 sources definitely show the reverse effect). These 47 sources all have FRII morphologies (Fanaroff & Riley 1974) and most are quasars, although a few radio galaxies are included. Very few FRII sources have detectable jets on both sides of the nucleus, and we will use the term "the jet" to refer to the brighter (in almost all cases the only) such feature. The most widely accepted explanation of the Laing–Garrington effect is that jets are intrinsically two-sided and relativistic: the nearer one appears brighter as a result of Doppler beaming and radiation from its lobe passes through less of the depolarizing medium around the source (Laing 1988; Garrington & Conway 1991). Thus the Laing–Garrington effect is explained as a consequence of orientation.

Liu & Pooley (1991) found that there is also a strong correlation between depolarization and lobe spectral index: the lobe with the flatter spectrum is the less depolarized. Their original sample contained a majority of sources without detectable jets, but 33 of the 47 sources with strong jets in Tables 3 to 6 of Garrington et al. also obey the Liu–Pooley rule.

Taken together these two strong correlations imply that the lobe spectrum is flatter on the jet side of a source. According to the standard model of an extragalactic radio source the lobe material is almost static relative to the host galaxy and therefore any motion of the lobe material is inadequate to account for significant differences between the lobe spectra as an orientation-related effect. Thus the two correlations together constitute a *prima facie* case against the standard model of 'Doppler-boosted' relativistic jets.

The most plausible defence is that intrinsic and orientation effects both operate:

(i) The Laing-Garrington sample includes only sources with detected (and, in most cases, prominent) jets. The majority are identified with quasars, which tend to have much

⋆ jdt@sintra.cc.fc.ul.pt

brighter jets than radio galaxies of the same total power. By contrast, the Liu-Pooley sample was not selected on jet emission, and consists chiefly of powerful radio galaxies. According to 'unified theories' of radio galaxies and quasars (Scheuer 1987; Barthel 1989), all of the sources form part of the same population, being classified as quasars if their jet axes are closer than $\approx 50^\circ$ to the line of sight, otherwise as radio galaxies. Faraday rotation and depolarization increase with the amount of ionized gas and magnetic field along the line of sight to the emitting region, and differences between the two lobes will result either from orientation or from intrinsic asymmetries in the surrounding material. Differences between the path lengths to the two lobes will be much larger for the quasars, and we might expect orientation effects to dominate. For the radio galaxies, on the other hand, path-length differences should be small, and intrinsic effects will be relatively more important.

(ii) For radio galaxies without strong jets, the shorter lobe is also the more depolarized, but this effect is barely significant in quasars (Laing 1993), despite the fact that the nearer lobe should appear longer as a result of differential light-travel effects (Ryle & Longair 1967). The shorter lobe in radio galaxies is also associated with brighter line-emitting gas (McCarthy et al. 1991), and this cannot be an orientation effect. We therefore require an intrinsic mechanism which relates lobe length, spectral index and depolarization, and which dominates in radio galaxies, together with an orientation-dependent mechanism which relates jet sidedness, spectral index and depolarization for quasars.

(iii) The most plausible explanation for a correlation between spectral index and jet sidedness is that the emission from a lobe might include significant contributions from the jet or an associated hotspot, both with flatter spectra than the surrounding material (Garrington et al. 1991; Tribble 1992). It is widely believed that the flow velocity of hotspot material is a substantial (though ill-defined) fraction of the speed of light (Blandford et al. 1984; Bridle & Perley 1984) and therefore that significant Doppler beaming should occur in hotspots.

If unified models are correct, then the intrinsic mechanism postulated for radio galaxies must also operate in quasars, in competition with orientation effects. Evidently what is needed is the direct observation of the spectral indices of the lobes of radio sources with jets, with enough resolution to discriminate clearly between lobe, jet and hotspot. In this paper we report detailed comparisons of the spectral index distributions in a small sample of quasars; a preliminary account based on the sources analysed at that time was given at the Mt. Stromlo symposium of 1993 (Bridle et al. 1994b). (Note, however, that Fig. 1 of that paper is incorrectly drawn: some sources have jet and counter-jet side labels reversed.)

1.2 Previous work

Garrington et al. (1991) mapped 47 quasars with jets, at 1.4 and 5 GHz, and found that in 37 out of 47 the side of the source with the jet had the flatter spectrum (see table 3 of that paper). These observations, then, show the direct correlation which challenges the standard model of 'Doppler-boosted' jets. However, as the authors themselves state, the images do not have enough angular resolution to permit further investigation of the causes of the correlation; in particular, in most cases they do not adequately resolve the hotspots from the relatively low-brightness lobes to allow the spectral index of the lobes to be measured reliably.

Barthel et al. (1988) and Lonsdale et al. (1993) made images of over 100 quasars, many of which were observed at both 5 and 15 GHz and also have clearly detected jets. So far as we know, these have not been investigated from the point of view of the present paper, and it is not clear that these data will lend themselves to measuring the distribution of spectral index in low-brightness regions.

Lonsdale and Morison (1983) find spectral asymmetries in the hotspots of four powerful radio sources. In two of these sources jets have now been detected (3C268.4 and 3C249.1; the latter is also in our sample); in these sources the hotspot spectrum is flatter on the jet side. In the other two sources the flatter spectrum is found in the more compact component, which is preferentially found on the jet side (Laing 1989; Bridle et al. 1994a).

Throughout this paper, we define the spectral index α in the sense flux density $\propto$ frequency$^{-\alpha}$.

2 OBSERVATIONS

2.1 The sample

Because we wish to explore spectral index distributions, we are restricted to a small sample of sources which are bright enough to be mapped in detail. We therefore started with the 12 quasars of which Bridle et al. (1994a, hereafter BHLBL) had already made detailed 5 GHz images, plus 3C47 (Fernini et al. 1991) which satisfies the same selection criteria and for which 5 GHz data of similar quality were available. The BHLBL sample was a subset of the 19 brightest quasars with angular size greater than 10 arcsec in the 3CR catalogue, the only further selection being for reasons of scheduling. Of these 13 quasars, we selected those with prominent one-sided jets and fairly standard appearance; thus we excluded 3C68.1 (ambiguous jet sidedness), 3C215 (jets on both sides of the core, and 90° distortion between smallest and largest scales) and 3C9 (because there is little of the source that can be described unequivocally as 'lobe' rather than 'jet').

2.2 Observing programme

In order to derive spectral-index maps, we made new observations at 1.4 and 1.7 GHz with MERLIN and the National Radio Astronomy Observatory (NRAO) VLA, and extracted additional data from the VLA archive. The 1.4–1.7 GHz observations were designed to provide as much overlap as possible in *uv* coverage with the 5 GHz observations of BHLBL. Most sources were just observed with the VLA in the A configuration, but 3C208 and 3C432 are only 14.6 and 14.8 arcsec in extent, respectively, so that even the VLA A array does not provide enough angular resolution; for these, MERLIN observations were obtained and combined with the VLA data. Observations of 3C351 at 1417.5 MHz in A array poorly covered the *uv* plane, and undersampled the large scale structure. For this reason the data were combined with

Table 1. Observing schedule

Source	Observing date	Duration	Array	Frequency (MHz)
3C47	1992 Dec 7	399m	VLA-A	1664.9, 1635.1
	1986 Jul 12	36m	VLA-B	1652.4
3C175	1992 Oct 31	89m	VLA-A	1417.5, 1467.5
3C204	1982 Mar 1	18m	VLA-A	1417.5
3C208	1981 Feb 24	19m	VLA-A	1464.9
	1994 Aug 14	14h	MERLIN	1420.0, 1658.8
3C263	1992 Oct 31	89m	VLA-A	1417.5, 1467.5
3C249.1	1982 Mar 1	38m	VLA-A	1417.5
3C334	1992 Oct 31	138m	VLA-A	1417.5, 1467.5
3C336	1992 Oct 31	47m	VLA-A	1417.5, 1467.5
3C351	1982 Mar 11	12m	VLA-A	1417.5
	1982 May 30	26m	VLA-A	1417.5
	1987 Nov 25	23m	VLA-B	1452.4,1502.4
	1987 Dec 2	6m	VLA-B	1452.4,1502.4
3C432	1992 Nov 1	90m	VLA-A	1464.9, 1514.9
	1994 Aug 1	14h	MERLIN	1420.0, 1658.8

B array observations. Table 1 shows a summary of the lower-frequency observations.

The VLA data were reduced and calibrated using the NRAO AIPS package. Initial editing and calibration of MERLIN data was performed using the OLAF package at Jodrell Bank, before being transferred to AIPS for self-calibration and imaging. Where possible only phase self-calibration was used. In a few cases with significant amplitude errors (for example when combining VLA and MERLIN data; see below) amplitude self-calibration was used with a long integration interval.

In order to maximise the *uv* coverage of the sparse MERLIN array, multi-frequency synthesis imaging was used (Conway et al. 1990). The data from the two frequencies were first corrected in total flux for the spectral index of the source and then combined to form a single data set. The spectral index correction was calculated using the compact components from the 5 GHz and one of the 1.4 or 1.7 GHz images. The dominant spectral errors will come from bright compact components (hotspots, core), yielding an error of $\approx I\alpha'/200$ near the hotspots, where I is the peak surface brightness and α' is the residual spectral index, i.e. the difference between the spectral index assumed for the purposes of correction and the true spectral index of the compact feature (Conway et al. 1990). The spectral errors will be below the level due to thermal noise and dynamic range limitations if the residual spectral index of the compact component is $\lesssim 0.15$. The residual spectral index is less than 0.15 near the hotspots; and in both sources imaged by this method, there is no lobe emission near the core, where larger errors might occur. Our images are therefore limited by 'reconstruction errors', not spectral errors and thus we are confident in using these images for the purposes of spectral index analysis. The MERLIN data were combined with the VLA data with weights proportional to the inverse expected rms noises on a single integration point. The combined data were then further calibrated, including a few passes of amplitude self-calibration.

Images at all frequencies were made using the AIPS CLEAN algorithms APCLN and MX. All images were CLEANed to the noise level to ensure that all significant emission, especially in the low brightness regions, was restored with the same effective resolution by CLEAN.

2.3 The 1.4 GHz images

The images are shown in Fig. 1. The contours are those used to divide the sources up into zones for the spectral index comparisons (see below): the lowest solid contour is at 3σ and the others are evenly spaced in log(surface brightness).

Table 2 shows the imaging parameters used and the total flux density in the images to the 3σ contour on the 1.4/1.7 GHz image. The single dish total flux densities used were the 1400, 2695 and 5000 MHz flux densities of Laing & Peacock (1980), interpolated to the observing frequency. Our L-band image of 3C334 apparently contains only 87 per cent of the single dish flux density, but the latter contains a contribution from another source of 114mJy 4.4 arcmin from 3C334 itself (as noted by BHLBL). Precisely how much that source contributed depends on details of how the single dish measurements were analyzed to allow for finite size, but it seems likely that most of the flux of the confusing source was included. Our image then contains 92 per cent of the corrected single-dish flux density. It is seen from Table 2 that we have a good representation of the total source flux density in all our other images. 3C351 has been imaged at a lower resolution than the other sources in order to show the extended region of low surface brightness preceding the N hotspots as this region was poorly represented at higher resolution.

2.4 The comparison between 1.4 GHz and 5 GHz images

As stated in the Introduction, we wish to compare the spectra of the lobes on the jet and counterjet sides, taking care to distinguish between lobes, hotspots and jets. Nevertheless we begin by noting that, when we compare the entire contents of the lobes, as in Garrington et al.(1991), the correlation found by these authors also appears in our data. Table 3 shows that in 7 cases out of 10 the jet side has the flatter spectrum, in two there is no significant difference and in one the jet side has the steeper spectrum. Thus the spectra of our sample are not atypical.

As soon as we try to compare the spectra of lobes (excluding jets and hotspots) a fundamental complication becomes obvious: there is no such thing as 'the spectral index of the lobe'. The spectrum steepens progressively (though usually not very regularly) from the neighbourhood of the hotspot towards the middle of the source (a trend generally attributed to synchrotron losses). Some scheme must be invented for comparing like with like on the two sides. One might consider comparing spectral indices at the same fractional distance from the core to the end of the lobe (or to the hotspot); that is not particularly satisfactory in practice as the lobes are often morphologically very different, they may have protrusions and the hotspots are often recessed from the end of the lobe. The scheme we have adopted is to compare regions with the same surface brightness. That brings certain complications with it (see e.g. Section 4.2) but other

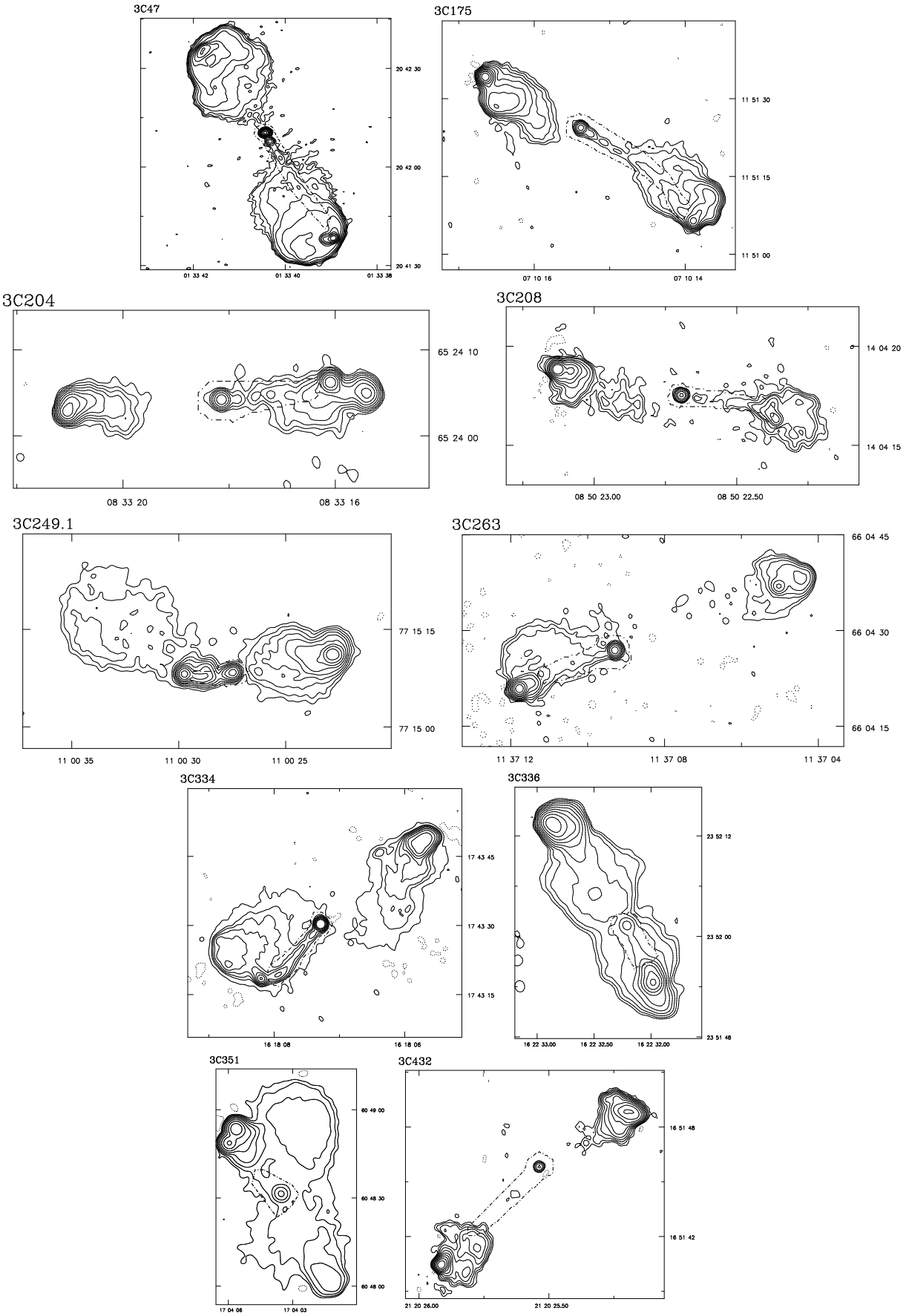

Figure 1. The 1.4/1.7 GHz images of the sample. The contours are those used to divide the sources into surface brightness regions and the dotted lines enclose the core and jet regions excluded from the spectral index calculations

Table 2. Image parameters

	FWHM	1.4/1.7 GHz noise (μJy/bm)	contour factor	total flux density (Jy)	% single dish flux density	4.86 GHz noise (μJy/bm)	total flux density (Jy)	% single dish flux density
3C47	1.45 x 1.13	48	1.96	3.36	93	35	1.22	111
3C175	1.30	151	2.01	2.53	105	38	0.67	100
3C204	1.15	199	1.91	1.19	89	61	0.32	93
3C208	0.35	250	1.92	2.16	104	25	0.56	102
3C249.1	1.20	242	1.87	2.33	104	32	0.81	101
3C263	1.10	197	2.20	3.15	103	57	1.11	105
3C334	1.30	73	1.80	1.83	87	36	0.63	106
3C336	1.25	187	2.00	2.63	99	38	0.82	115
3C351	3.00	222	3.49	3.13	90	105	1.18	96
3C432	0.37	234	1.76	1.46	104	19	0.37	114

Table 3. Total lobe spectral indices, determined from the ratio of flux densities inside the 3σ contour on the 1.4/1.7 GHz image and the identical region in the 5 GHz image. Cores have been excluded.

Source	α^{js}	α^{cjs}
3C47	0.85	0.94
3C175	1.07	1.15
3C204	1.14	1.19
3C208	1.14	1.25
3C249.1	0.86	0.96
3C263	0.96	0.88
3C334	0.99	1.00
3C336	0.96	0.98
3C351	0.78	0.88
3C432	1.05	1.28

(js) refers to jet side;
(cjs) to counter-jet side.

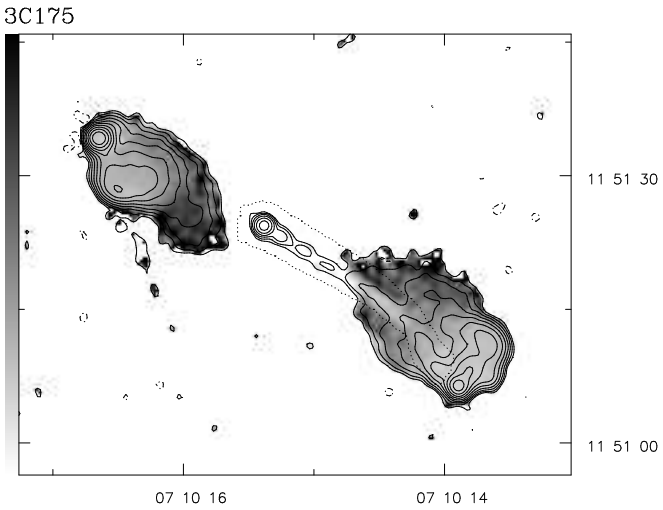

Figure 2. Subdivision of 3C175 into surface brightness zones. The contours are spaced as for the spectral index calculations on the 1.4 GHz image and the grey scale represents the spectral index between 1.4 and 5.0 GHz. The dotted line again shows the excluded jet and core region. Contours : -.465, .465, .931, 1.865, 7.479, 14.96, 30.00, 60.08, 120.3, 241.0 mJy/beam. Grey scale: 0.6 (white) – 2.5 (black)

schemes that we considered were much less satisfactory, and the adopted scheme at least has the merit of leading to an interesting result (Section 3). The analysis therefore proceeds as follows:

(i) Make 5 GHz and 1.4/1.7 GHz images at the same angular resolution, using as near as possible the same *uv* coverage; the authors of BHLBL kindly made the calibrated 5 GHz visibilities available. Correct the images for any zero-level offsets using estimates of the mean off-source level.

(ii) Cut out the region of the jet and the core; the excluded regions are indicated in Fig. 1.

(iii) Subdivide the resulting images into regions within fairly narrow ranges of surface brightness at 1.4 or 1.7 GHz. The ranges of surface brightness were chosen as follows: the lowest contour was set at three times the rms noise level on the 1.4 or 1.7 GHz image, and the image was divided into logarithmically equally spaced contours. Each source was divided into about 10 zones; the precise number depends on the dynamic range and was chosen so that each zone contains a sufficiently large number of beams to ensure that the spectral error introduced by the thermal noise is small, and so that the zone is generally wider than a beam. The contours shown in Fig. 1 are the contours dividing the zones. Fig. 2 shows the same contours for 3C175, but with a grey scale of spectral index superposed. This demonstrates that surface brightness and spectral index are roughly correlated.

(iv) Compute the spectral index for each surface brightness range on each side of the source from the ratio of the total flux densities in that surface brightness range at 5 GHz and 1.4/1.7 GHz. Every effort was made to remove any small zero-level offsets from the images but note that the *differences* between the spectra on the two sides of a source, at the same surface brightness, are in any case insensitive to such errors, and are unaffected by inaccuracies in the flux scale.

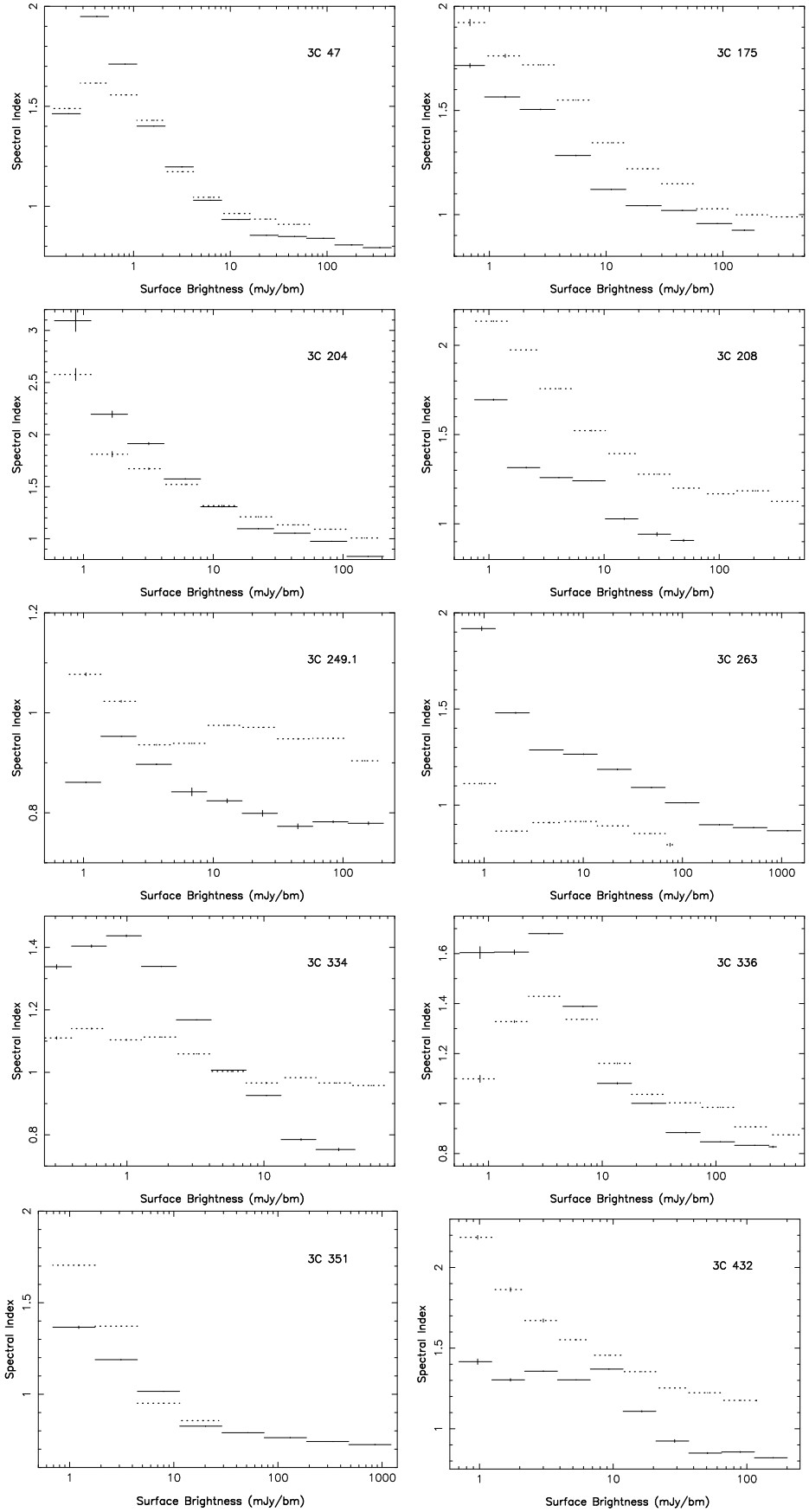

Figure 3. Plots of 1.4/1.7 to 5.0 GHz spectral index versus surface brightness for the jet and the counter-jet side of each source in the sample. Counter-jet side: dotted lines. Jet side: continuous lines.

3 RESULTS

Fig. 3 shows the spectral indices for both sides of each source plotted against surface brightness. In each diagram the length of a horizontal line shows the range of surface brightness spanned by the zone. The vertical lines indicate the formal errors due to the noise levels in the images at both frequencies.

The systematic errors in spectral index are less well determined. Small errors in the reconstruction algorithms were investigated by making images by a 'maximum entropy' algorithm (VTESS), or by using different parameters in the CLEAN algorithms. These tests typically indicated an uncertainty comparable to the errors due to the noise in the regions of highest surface brightness, increasing to $\sim 0.1-0.3$ in the region of lowest surface brightness. In all cases however, the effect was, as expected, the same for both the jet side and counter-jet side, thus not affecting our conclusions.

With the single exception of 3C263, the plots show that the high surface brightness regions have flatter spectra on the jet side. The spectral differences in the low-brightness regions show no obvious pattern in these plots alone, but we noticed that 3C263, the one source which breaks the rule at high surface brightness, is strikingly asymmetric. This led to the discovery that the spectral index difference in the low-brightness regions correlates strongly with the length of the lobe: the longer lobe has the flatter spectrum. The extent to which our data support these assertions is illustrated in Fig. 4. In this figure the lobe length ratio has been calculated using the distance from the core to the furthest 3σ contour. (Using the definition of distance from the core, through the hotspot to the the furthest 3σ contour 3C249.1 has a ratio of jet-side to counterjet-side lengths of 0.6, but the figures for all other sources are only slightly changed, and no other sources show a change in the sense of the asymmetry.)

Fig. 4a shows that for all sources, except 3C263, the jet side spectra in the highest surface brightness regions of the source are consistently flatter than their counterparts on the counter-jet side (i.e. they fall below the dotted line). As some of the sources have a substantial peak brightness asymmetry the highest bins are often found only on one side. To create properly paired highest bins we adopted the following procedure: on both sides we summed all the flux above the lower surface brightness bound of the top bin on the side with the lower peak surface brightness. As can be seen from inspection of Fig. 3, because of the magnitude of the differences, other sensible ways of pairing the bins would have left the conclusions unchanged. 3C351 has a large peak surface brightness asymmetry, and only four paired surface brightness bins. For this source we have included only the two highest surface brightness bins in Fig. 4.

Fig. 4b shows a strong dependence of the spectral asymmetry in low-brightness regions, not on jet side, but on length of lobe. This is evident from the fact that nearly all the points lie in the second and fourth quadrants of the diagram. Thus when the jet side is longer (right of dotted line), the jet side has a flatter spectrum (below dotted line), but when it is shorter it has a steeper spectrum. The flatter spectrum is found on the longer side in all sources except 3C47.

The probability that at least 9 out of 10 sources have flatter spectra on the jet side by pure chance is 1%. (For a two-tailed distribution, i.e. either $\geq 9/10$ or $\leq 1/10$, the probability is 2%.) The formal statistical significance is not great, but we note that in the one exception, 3C263, the jetted lobe is very much shorter than the unjetted lobe, so the factors related to lobe length may well dominate in this source. If we exclude 3C263, the probablity for 9/9 sources is 0.2% (0.4% 2-tailed). The probability that 8 out of 9 sources follow the lobe-length relation of Figure 4(b) by pure chance is 2% (4% 2-tailed). These probabilities follow directly from the binomial distribution.

For completeness, we also note that the Laing-Garrington effect for our sample is found in 7/10 of our sources: the exceptions are two sources showing very little asymmetry (3C263 and 3C249.1) and one (3C204) apparently showing the reverse effect (although the source is almost completely depolarized by 1.5 GHz so measurement of the asymmetry is difficult).

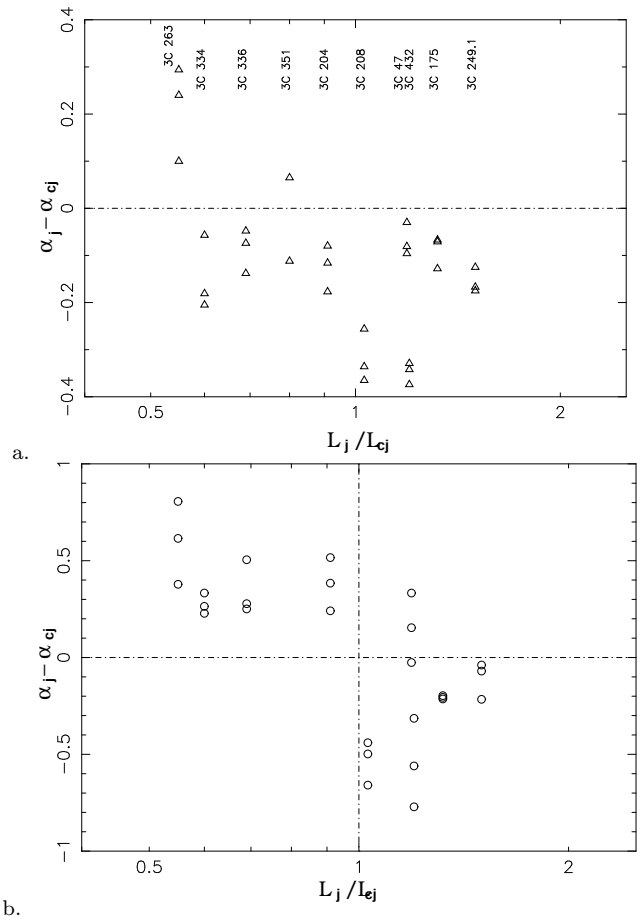

Figure 4. The spectral indices of low and high surface brightness regions related to jet side and lobe length. Figs. 4a and 4b show spectral index differences between the jet and counter-jet lobes of each source for the highest and lowest three surface brightness bins, respectively. The spectral indices of the jet and counter-jet lobes are α_j and α_{cj}, respectively, and their lengths are L_j and L_{cj}.

4 INTERPRETATION

In this section we discuss various attempts to explain the two correlations presented in the previous section, and eliminate as many as we can.

4.1 Jet side and α in bright regions

The hotspot on the approaching (jet) side may make a larger contribution to the spectral index of the high-brightness regions than its counterpart in the receding lobe as a result of Doppler beaming (e.g. Tribble 1992); this is perhaps the simplest model for a sytematically flatter spectrum on the jet side. However, the simplest models of this type fail to explain the present observations, in which regions of the same surface brightness were compared. (This applies to all models based on different ratios of flat- and steep-spectrum power-law components, regardless of how difference in ratio is achieved.) Consider a model with a steep spectrum background of uniform surface brightness on which are superposed flat-spectrum hot-spots of different intensities (and shapes) on the two sides: points with the same suface brightness will then have the same spectrum. (This is true regardless of angular resolution.) Certain more complicated models may produce the desired effect; for example, a background symmetric about the nucleus, peaking under similar-sized hot-spots, would produce a flatter spectrum at the brighter hot-spot when comparing regions of equal surface brightness. However, modifying the symmetry and shape of the background distribution, or the relative sizes of the hotspot will not generally give the same result.

Another way to obtain a spectral index asymmetry in a relativistically-expanding source would be to postulate that the intrinsic spectrum is curved and that the asymmetry is produced by the Doppler shift. If the spectral index increases with frequency, and the approaching lobe is seen at a significantly lower emitted frequency, an asymmetry of the right sense could be produced. This mechanism could operate in smaller regions with significant flow velocities such as hotspots. A calculation using theoretical 'single burst' spectra with injection spectral index of 0.5 shows that a velocity of $\approx 0.3c$ at 30° to the line of sight (and correspondingly smaller speeds at smaller angles) is enough to cause the observed effect, if the relativistic component dominates the hotspot spectrum, and the curvature is due to synchroton ageing of an initial power-law electron population. The less curved 'continuous injection' spectra require somewhat higher speeds to explain the correlation. Observational evidence for curved hotspot spectra at high resolution comes from Cygnus A (Carilli et al. 1991), but adequate resolution over a large frequency range is available for few other sources (Meisenheimer et al. 1989), and in particular for none of our sample.

We have tested the hypothesis that the spectral differences between high-brightness regions are due to high flow velocities in the hotspots in two ways, as follows:

(i) Table 4 lists the flux densities of the hotspots in our sample. We present two sets of hotspot flux densities, that of BHLBL (obtained by a well-defined, though arbitrary set of rules defining a hotspot) and our own estimates (for which the hotspots were chosen subjectively). In most cases our estimate of total hotspot flux density is close to that of BHLBL, but in a few cases there is obvious disagreement, as on the counter-jet side of 3C432 where different features have been chosen in the two cases. In the majority of the sources there is a good case for asserting that the jet-side hotspot is the brighter of the two, but there are striking exceptions — 3C175, 3C208, 3C336 — whichever set of hotspot criteria is used. In such sources the flatter spectrum on the jet side obviously cannot be blamed on a greater flat spectrum contribution from the hotspot. Thus, although relativistic flux–boosting of a flat–spectrum hotspot in a steeper spectrum lobe could potentially account for the effect, it clearly cannot do so in all cases. The inclusion of two sets of flux density estimates emphasises that these conclusions are robust and insensitive to details of hotspot definitions.

Table 4. 5 GHz flux densities of hotspots in mJy.

Source	S_j^{tot}	S_{cj}^{tot}	S_j^{tot}	S_{cj}^{tot}	S_j^{peak}	S_{cj}^{peak}
	BHLBL		our estimates			
3C47	268	-	257	-	198	25
3C175	64	152	62	138	25	65
3C204	61	42	60	40	43	30
3C208	28	203	36	198	21	139
3C249.1	86	188	80	120	48	18
3C263	528	21	500	23	330	13
3C334	20	-	18	-	6	3
3C336	95	254	95	280	50	40
3C351	201	-	202	5	156	1
3C432	105	6	103	280	73	34

(ii) The two effects of high flow velocity (the Doppler effect shifting a curved spectrum in frequency and the relativistic flux-boosting of the approaching flow) may be thought of as increasing the proportion of flat-spectrum component in the jet-side hotspot. Even if the fast flow is confined to the hotspot, it might be suspected that, at the resolution used for the spectral-index analysis, beam smearing could spread a flatter spectrum from the hotspot to adjacent regions of somewhat lower surface brightness.

To test the possibility that the effect is solely due to a single compact hotspot, we used the three sources in which the spectral index difference $\alpha_j - \alpha_{cj}$ reverses between high- and low-surface-brightness regions (3C204, 3C334 and 3C336). If the above suspicion were well-founded, artificial spectral steepening of the jet-side hotspot spectrum alone should remove the correlation between jet side and flat spectrum. The jet-side hotspot was modelled using the 2D Gaussian fit to the high resolution image of the hotspot at 5 GHz made by BHLBL. This fitted hotspot was convolved down to the resolution of our spectral analysis. This model was then used to remove 5 GHz flux progressively from the site of the high resolution fit to the hotspot. Even when the amount of flux subtracted from the hotspot was large enough to produce a spectrum of the compact component which was steeper than that on the counter-jet side, there still remained a region of intermediate brightness which was largely unaffected by the changes to the hotspot, and which retained its flatter spectrum. Fig. 5 shows the results for a typical source (3C334). Thus it is clear that "contamination" of the intermediate surface brightness regions by an insufficiently resolved flat

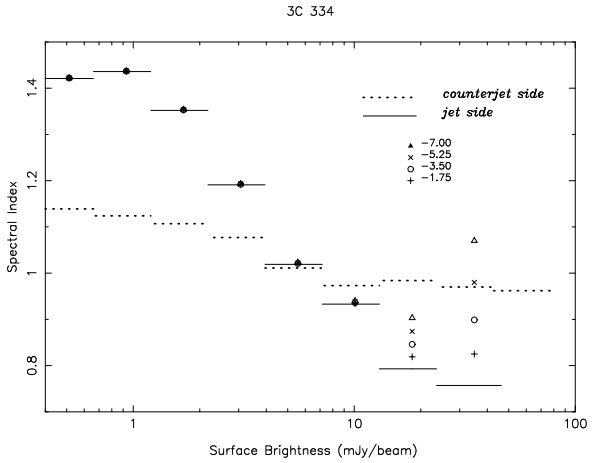

Figure 5. The effects of removing a flat spectrum component from the jet-side hotspot in 3C334. The symbols indicate results after subtraction of 5 GHz flux. Horizontal binning bars are omitted for clarity; the flux subtracted is indicated in mJy in the legend. As progressively more flux is subtracted from the jet side hotspot, its spectrum necessarily becomes progressively steeper, but the intermediate surface brightness regions on the jet side still have flatter spectra.

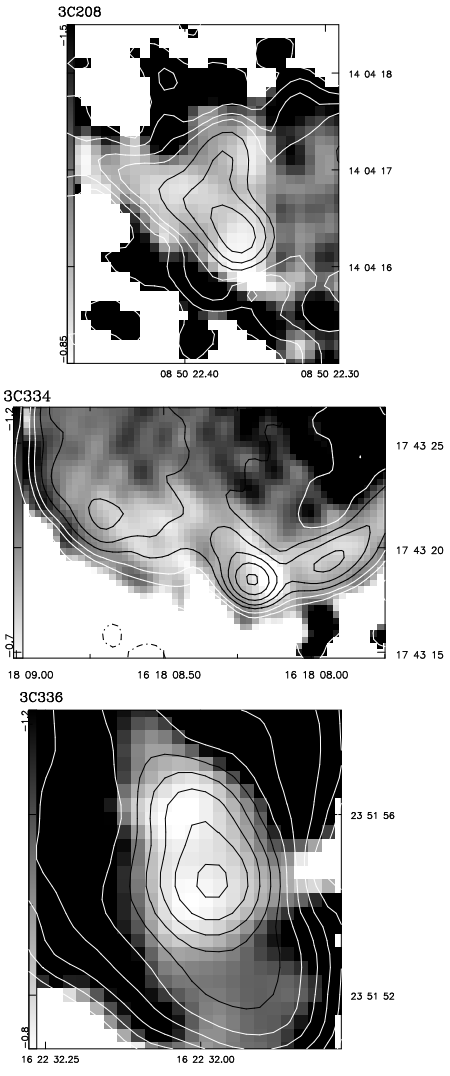

Figure 6. Detail of jet side lobes of 3C 208, 3C 334 and 3C 336. Grey scale representations of spectral index are superposed on total intensity contours.

spectrum hotspot is not enough on its own to account for the observations.

We conclude that, if relativistic motion is responsible for the spectral index asymmetry, then the fast forward flow is not confined to a single compact hotspot. What regions, then, might take part in this forward motion? It is well known that many sources have double or even multiple hotspots (3C351 is a striking example, and in the present sample 3C175, 3C334, 3C336 and 3C432 show double hotspots at higher resolution), but that by itself does not explain why there should be fast forward motion in both. One possibility is that the point of impact of the jet on the shocked intergalactic medium is recessed (i.e. not at the extreme end of the lobe) and fast flow continues beyond the initial hotspot, as the images of 3C204, 3C334 and 3C336 might indicate (Fig. 1). Inspection of the spectral index image for 3C334 shows that a ridge with relatively flat spectrum indeed extends along the ridge of high surface brightness beyond the hotspot (Fig. 6b). At higher resolution (BHLBL), the hotspot of 3C336 (single in our images) divides into two compact bright features. These coincide with two flatter-spectrum regions in Fig. 6c. 3C208 also has a recessed hotspot on the jet side, but in that case the flattest spectra occur on the hotspot and on a region extending northward from it (Fig. 6a), at about the same distance from the quasar. This suggests that the jet has split before reaching the hotspot, or perhaps that one of the flat-spectrum regions represents an earlier hotspot, now detached from the jet but still being fed with high-speed material, as in the numerical simulations of Cox, Gull & Scheuer (1991). It is also possible that projection effects have transformed a gentle bend in the flow into a sharp ($> 90°$) change of direction, but that would imply a very small angle of source axis to line of sight, and a correspondingly large true aspect ratio for the source. Like 3C334 and 3C336, 3C47 and 3C175 show relatively flat spectra along high surface brightness ridges extending out of the jet-side hotspots, but in these sources the flow seems to turn through a (projected) right angle at the hotspot. Perhaps these flows have more in common with what is going on in 3C208 than with flows in 3C334 and 3C336.

Numerical simulations of radio emission from hotspots generated by relativistic jets have so far been restricted to the axisymmetric case. Komissarov & Falle (1996) find that the brightness distribution of the approaching hotspot is dominated by the conical termination shock, whilst the emission from the receding hotspot comes mainly from the high-pressure part of the backflow, and is therefore limb-brightened. High-resolution non-relativistic simulations of Norman (1996), suggest that there is a region of supersonic turbulence near the leading edge of the source (extending 4–5 lobe radii in these simulations) in which the jet is violently deflected. The jet can therefore impinge obliquely on the contact discontinuity to produce a deflected or wall jet (Williams & Gull 1985; Wilson 1989; Cox, Gull & Scheuer

1991; Norman & Balsara 1992). These deflected flows are morphologically very similar to the flat-spectrum features observed in sources such as 3C334. A key feature of these simulations, from our point of view, is that they lead to oblique shocks and therefore to relatively large forward velocities, so that significant beaming can occur over much of the post-shock flow, especially when the hotspot is recessed.

The simulations also indicate that the observations of the approaching and receding hotspots may well be dominated by different parts of the flow, and might then have different spectra. Observationally, the more diffuse appearance of the counterjet-side hotspots also supports this idea.

4.2 The length of the lobe and α in lower brightness regions

The expansion velocities of the low-brightness regions are unlikely to exceed a few per cent of c (Scheuer 1995), so it is difficult to see how beaming effects could account for large-scale spectral asymmetries, even if the intrinsic spectra are curved. Two obvious possible causes of the correlation of the continuum radio spectra with the size of the radio lobe are synchrotron loss and adiabatic expansion. We consider these in turn below.

(i) Synchrotron losses

Other things being equal, the break frequency due to synchrotron loss varies as B^{-3} (B = magnetic flux density). The equipartition estimate of B varies as (linear size)$^{-6/7}$, for given radio power. If, on the other hand, the magnetic field in the larger lobe is simply a homologously expanded copy of that in the smaller lobe, then $B \propto$ (linear size)$^{-2}$. In either case, the break frequency depends sensitively on linear size, and this dependence would produce a higher break frequency (and hence a flatter spectrum over a fixed frequency interval) in the larger lobe, i.e. a correlation in the sense that is observed. The theoretical predictions are more complicated if we compare regions of equal surface brightness in the two lobes, but in essence the result remains the same.

Blundell and Alexander (1994) pursued this line of argument to explain the correlation between jet side and flatter spectrum. They argued that the near (jet) side is observed at a later stage of development (owing to light travel time effects), and is therefore the larger. While we cannot accept that part of their hypothesis, because the longer lobe is on the *counter-jet* side in 5 of our 10 sources, the strong dependence of synchrotron loss on linear size remains a plausible explanation for spectral asymmetries in low-brightness regions.

(ii) Adiabatic losses.

The observation of spectral index gradients in the lobes indicates that individual regions have spectra steepening with frequency, possibly because of synchrotron losses (this need not conflict with a fairly straight spectrum for the whole source as many sources are dominated by radiation from hotspots where very little synchrotron loss has occurred at frequencies less than $\sim$ 10 GHz). We now ask how different amounts of expansion in the two lobes, acting on these curved spectra, might affect the differences between their observed spectral indices.

To isolate the effects of expansion, consider a simple model: two lobes were identical initially; then one expanded adiabatically by a linear factor R which is a little greater than 1. The magnetic field in the larger lobe becomes R^{-2} of the field in the corresponding bit of the smaller lobe, and the electron energy distribution is shifted downwards (electron energy $\propto R^{-1}$), with the result that the entire spectrum is shifted downwards in frequency by a factor R^{-4}. Thus we should expect the larger lobe to have a spectrum that is steeper over the same frequency range. This is the reverse of the correlation observed in Fig. 4. Closer consideration (below) modifies that conclusion, for we must remember that we compare regions of equal surface brightness on the two sides.

Suppose that a certain region of the smaller lobe has spectral index α and surface brightness S/Ω. The corresponding region in the larger lobe has spectral index

$$\alpha' = \alpha + 4 \log R \frac{d\alpha}{d(\log \nu)}$$

and surface brightness given by

$$\log(S/\Omega)' = \log(S/\Omega) - 4(1+\alpha)\log R.$$

Therefore a region of surface brightness S/Ω, in the larger lobe, is expected to have spectral index

$$\begin{aligned} \alpha'' &= \alpha' + 4(1+\alpha)\log R \frac{d\alpha}{d(\log S/\Omega)} \\ &= \alpha + 4 \log R \left(\frac{d\alpha}{d(\log \nu)} + (1+\alpha)\frac{d\alpha}{d(\log S/\Omega)} \right) \end{aligned} \quad (1)$$

The last term is negative: brighter patches of source have flatter spectra. Thus we expect the larger lobe to have a flatter spectrum *for regions of equal surface brightness* if

$$\left| (1+\alpha)\frac{d\alpha}{d(\log S/\Omega)} \right| > \frac{d\alpha}{d(\log \nu)}$$

If we assume that the spectral gradient along the source is due to synchrotron losses we can evaluate the importance of adiabatic loss as an explanation for the observed correlation. We can calculate $\frac{d\alpha}{d(\log \nu)}$ as a function of α from the synchrotron spectrum of a given theoretical electron energy distribution. The results are shown in Fig. 7, which shows the results for two values of injection index for the case of a sharp energy cut-off. Another energy distribution of interest, that with no pitch–angle scattering of the electrons (Kardashev 1962), follows the above case closely, until α approaches $\frac{4}{3}\alpha_{injection} + 1$, which is the maximum spectral index possible in this model, so that $\frac{d\alpha}{d(\log \nu)} \rightarrow 0$. $\frac{d\alpha}{d(\log S/\Omega)}$ has to be estimated directly from our observations, as it involves the whole histories of synchrotron losses in different parts of the source.

The results are illustrated in Fig. 7. One point is plotted for each source. The value of α is taken as the mean of the three lowest surface brightness bins in the larger lobe. Errors in α are taken as the difference between the maximum and mean values of α in the lowest three bins.

The points need to fall above the line for adiabatic expansion to explain the observed correlation. It can be seen that this is indeed the case for most of the sources and two reasonable models of $\frac{d\alpha}{d(\log \nu)}$. We conclude that adiabatic expansion may contribute to the observed correlation.

It seems desirable to check the prediction that the larger

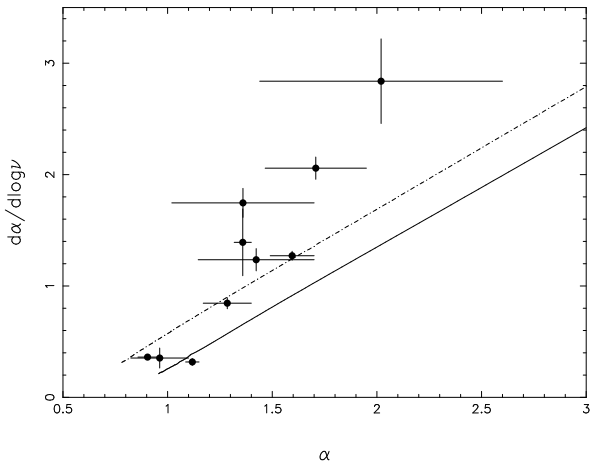

Figure 7. Calculated values of $\frac{d\alpha}{d(log\nu)}$ and observed values of $(\alpha+1)|\frac{\Delta\alpha}{\Delta\log(S/\Omega)}|$ plotted on the same scale. The lines are $\frac{d\alpha}{d(log\nu)}$ calculated for energy spectra with a sharp energy cut–off, and injection spectral indices of 0.5(dotted line) and 0.75(solid line). One observed point, from the longer lobe, is plotted for each source.

lobe *as a whole* has the steeper spectrum, but it is not clear how to do so. The difficulty is to identify which material is potentially affected by orientation-dependent effects. We have shown that such effects are not restricted to easily-identifiable regions such as hot-spots, and therefore that setting an intensity threshold will not unambiguously separate them.

5 CONCLUSIONS

In a sample of ten high-powered radio quasars we have found the following correlations:

(i) In regions of high surface brightness the radio spectrum is flatter on the jet side (9/10)

(ii) In regions of low surface brightness the radio spectrum is flatter on the long side (8/9)

If jet sidedness is a manifestation of relativistic flow, as is commonly believed, then the strong correlation (9/10 sources) found here between the spectral index of the hotspot and the jet side indicates that the spectral difference between the two sides is also a relativistic effect. We have also demonstrated that the correlation of flatter spectrum with jet side is not confined to the hotspot. Nevertheless, the correlation is presumably an orientation-dependent phenomenon, and we conclude that forward motion at a significant fraction of c also occurs in regions less conspicuous than that normally selected as 'the hotspot'.

We have argued that the observed correlation cannot result from a flat-spectrum component whose contribution to the hotspot is enhanced by forward beaming. Doppler frequency shifting of a curved hotspot spectrum might be able to explain the correlation. This would require flow speeds in excess of $0.3c$. A further possibility is that we are viewing different physical parts of the flow on the two sides as a result of Doppler enhancement and suppression of the post-shock flow.

The correlation of lobe length and radio spectrum has yet to be fully understood. One simple explanation is that it is due to differences in synchrotron losses in lobes of different volumes. Expansion losses may also play a role. The spectral asymmetry in the low surface brightness regions can be interpreted as an environmental effect due to the surrounding ambient gas containing the lobes. In this context, we note that the one source (3C 263) which disobeys the high surface brightness correlation also shows surprisingly little depolarization asymmetry. This and the fact that the jet side is only $\sim$ half the length of the counter-jet side indicates that the source may be confined by a denser medium on the jet side. In this case it may be that environmental effects produce the spectral-index and depolarization behaviour. Hall et al. (1995) indeed find evidence for an X–ray emitting clump associated with the short lobe of this source.

A similar study of a sample of nearby radio galaxies (in which environmental effects are expected to dominate) is now under way.

ACKNOWLEDGEMENTS

JDT, RAL and PAGS would like to thank the NRAO for hospitality. JDT thanks the British taxpayers for their assistance in the form of a PPARC studentship. The NRAO is a facility of the National Science Foundation, operated under cooperative agreement by Associated Universities, Inc. MERLIN is a national facility operated by the University of Manchester on behalf of PPARC.

REFERENCES

Barthel P.D., 1989, ApJ, 336, 606
Barthel P.D., Miley G.K., Schilizzi R.T., Lonsdale C., 1988, A&AS, 73, 515
Blandford M.C., Begelman R.D., Rees M. J., 1984, Rev. Mod. Phys., 56, 255
Blundell K. M., Alexander P., 1994, MNRAS, 267, 241
Bridle A. H., Perley R. A., 1984, ARA&A, 22, 319
Bridle A.H., Hough D.H., Lonsdale C.J., Burns J.O., Laing R.A., 1994a, AJ, 108, 766 (BHLBL)
Bridle A. H., Laing R. A., Scheuer P. A. G., Turner S., 1994b, in Bicknell G. V., Dopita M. A., Quinn P.J., eds., The First Stromlo Symposium: The Physics of Active Galaxies, ASP conference series Vol. 54, Astr. Soc. Pacific, San Francisco, p. 187
Carilli C. L., Perley R. A., Dreher J. W., Leahy J.P., 1991, ApJ, 383, 554
Conway J.E., Cornwell T.J., Wilkinson P.N., 1990, MNRAS, 246, 490
Cox C.I., Gull S.F., Scheuer P.A.G., 1991, MNRAS, 252, 558
Fanaroff B.L., Riley J.M., 1974, MNRAS, 167, 31P
Fernini I., Leahy J. P. Burns J. O., Basart J.P., 1991, ApJ, 381, 63
Garrington S. T., Leahy J. P., Conway R. G., Laing R. A., 1988. Nat, 331, 147
Garrington S.T., Conway R. G., 1991, MNRAS, 250, 198
Garrington S.T., Conway R.G., Leahy J.P. 1991, MNRAS, 250, 171
Hall P.B., Ellingson E., Green R.F., Yee H.K.C., 1995, AJ, 110, 513
Kardashev N.S., 1962, Ast. Zh., 39, 393
Komissarov S.S., Falle S.A.E.G., 1996, in Hardee, P.E., Bridle,

A.H. & Zensus, J.A., eds., Energy Transport in Radio Galaxies and Quasars, ASP conference series Vol. 100, Astr. Soc. Pacific, San Francisco, p. 327
Laing R. A., 1988, Nat, 331, 149
Laing R. A., Peacock J. A., 1980, MNRAS, 190, 903
Laing R. A., 1989, in Meisenheimer K. & Röser H.-J. eds., Hot-Spots in Extragalactic Radio Sources, Lecture Notes on Physics 327, Springer-Verlag, Berlin, p.95
Laing R.A., 1993, in Burgarella, D., Livio, M. & O'Dea, C.P., eds., Astrophysical Jets, Space Telescope Science Institute Symposium Series 6, Cambridge University Press, Cambridge, p. 95
Liu R., Pooley G. G., 1991, MNRAS, 249, 343
Lonsdale C.J., Morison I., 1983, MNRAS, 203, 833
Lonsdale C., Barthel P. D., Miley G. K., 1993, A&AS, 105, 91
McCarthy P.J., van Breugel W.J.M., Kapahi V.K., 1991, ApJ, 371, 478
Meisenheimer K., Röser H.-J., Hiltner P.R., Yates M.G., Longair M.S., Chini R., Perley R.A., 1989, A&A, 219, 63
Norman M. L., 1996, in Hardee, P.E., Bridle, A.H. & Zensus, J.A., eds., Energy Transport in Radio Galaxies and Quasars, ASP conference series Vol. 100, Astr. Soc. Pacific, San Francisco, p. 319
Norman M.L., Balsara D.S., 1992, in Röser H.-J. & Meisenheimer K., eds., Jets in Extragalactic Radio Sources, Lecture Notes on Physics 421, Springer-Verlag, Berlin, p. 229
Ryle M, Longair M., 1967, MNRAS, 123, 436
Scheuer P.A.G., 1987, in Zensus, J.A. & Pearson, T.J. eds., Superluminal Radio Sources, Cambridge University Press, Cambridge, p. 104
Scheuer P.A.G., 1995, MNRAS, 277, 331
Tribble P., 1992, MNRAS, 256, 281
Williams, A.G., Gull, S.F., 1985, Nat, 313, 34
Wilson M.J., 1989, in Meisenheimer K. & Röser H.-J. eds., Hot-Spots in Extragalactic Radio Sources, Lecture Notes on Physics 327, Springer-Verlag, Berlin, p. 215